SIMULATION OF A SHOCK WAVE INTERACTION WITH A BOUNDED INHOMOGENEOUS GAS–PARTICLE LAYER USING THE HYBRID LARGE-PARTICLE METHOD

D. V. Sadin[1], I. O. Golikov[2], and V. A. Davidchuk[3]

The problems of shock wave interaction with a bounded layer of gas suspension is studied in the case when a square-section inhomogeneity of reduced or increased density is situated inside this layer. The hybrid large-particle method of the second-order approximation in space and time is used for calculations. The numerical correctness of discontinuous solutions, in particular jumps of porosity, is confirmed by comparison with the asymptotically exact profiles of the mixture density. Analytical dependences of shock wave attenuation by a gas suspension layer are given. Shock-wave structures in two-dimensional regions and the effect of relaxation processes on them are analyzed.

1. Introduction. Unsteady flow of gas suspensions with shock waves and contact discontinuities are of practical interest in a number of applications related to spraying technologies, production of solid fuel rocket boosters, gas transport of bulk materials, assessment of potential consequences at explosive production facilities, protection of items by disperse barrier formations, etc.

Numerical modeling of non-equilibrium flows of gas mixed with particles encounters a number of fundamental difficulties, for example, in comparison with classical computational fluid dynamics. One of these factors is the non-conservative nature of the subsystems of the phase momentum equations associated with the change in the gas flow tube (the Archimedes force): $p\nabla\alpha_1$, where p is the gas pressure and α_1 is its volume fraction. No transformations have been found to date that would lead the conservation laws of two-phase media expressed in a sufficiently general form to a divergent form of notation. Conservativity has been achieved for a special case described by Rozhdestvensky and Yanenko [1] with regard to the conservation laws for the systems of two-phase medium equations [2]. In some works, the gas suspension dynamics are formulated in divergent form by neglecting the Archimedes force in the gas phase equations [3, 4], which seems to be true for small porosity gradients. We must note that the non-conservativity problem arises primarily for discrete models that require a fully divergent flow notation of the equations and rely on a characteristic representation and on the solution of the discontinuity decomposition problem (the Riemann solvers) [5–7].

In various mathematical formulations of non-equilibrium gas suspension dynamics, the gas and particles each have their own velocities and temperatures, including an equal pressure term [8–10] or two pressure terms for each phase [11–13]. In the disperse phase, the pressure arises as a result of random collisions of particles in motion, like in the kinetic molecular theory of gases. The problem of mathematical description of chaotic motion of particles in a carrier gas remains open up to date. Gol'dshtik [14] proposed a mechanism for generating a "boiling" particle layer due to the action of Magnus forces. Further, in [15, 16] the authors considered the physical effects of vortex flows around disperse particles resulting from longitudinal and transverse force fluctuations at Reynolds phase slip number $\mathrm{Re}_{12} > 200$. Kinetic molecular approaches to describing dynamic processes in colliding media are developed in [3, 4, 11–14, 17, 18]. Collision-free models of the "dusty" gas and some systems of equation systems describing the motion with two pressure terms are non-hyperbolic in the general case [19–21]. The conservation laws of two-phase media of hyperbolic type are applied and developed in a number of

[1] Mozhaisky Military Space Academy, ulitsa Zhdanovskaya 13, St. Petersburg, 197198, Russia; Dr. Sci., Professor, e-mail: sadin@yandex.ru

[2] Mozhaisky Military Space Academy, ulitsa Zhdanovskaya 13, St. Petersburg, 197198, Russia; Ph.D., Associate Professor, e-mail: igira55@yandex.ru

[3] Mozhaisky Military Space Academy, ulitsa Zhdanovskaya 13, St. Petersburg, 197198, Russia; Postgraduate, e-mail: david_lxii@mail.ru

studies [5–7, 22, 23]. The consideration of inertial effects (the added mass forces) in the flow of dispersed particles leads to a "non-classical" characteristic representation of the conservation laws [24].

Another problem in the computational dynamics of heterogeneous media is related to stiffness, i.e., to a substantial difference in the characteristic temporal scales when the phase relaxation times are much shorter than the gas dynamic scale of perturbation propagation within the computational cell. A number of highly stable discrete models are proposed for meaningful formulations of problems [25–30]. One the useful computational properties of the scheme is its K-stability [31, 32]. The informal meaning of this property is that the stability is determined only by the gas dynamic scale of the discrete problem (the Courant–Friedrichs–Lewy condition) and does not depend on the phase relaxation times. In the case of intense phase interaction, traditional discrete models are no longer applicable because of unacceptably small time steps.

The interaction between a shock wave and a layer or cloud of gas with suspended particles is studied in [33–37]. Our study considers the shock wave motion in a porosity discontinuity medium. We analyze the accuracy of the hybrid large-particle method and the convergence of the numerical solution to an asymptotically exact equilibrium solution for small dispersed particle sizes. The problems of refraction of an incident shock wave on square cross-sectional heterogeneities with reduced or increased density are studied in two-dimensional regions.

2. Basic equations. Let us consider the conservation laws for a calorically perfect gas and solid incompressible particles in the multifluid formulation [30]:

$$\frac{\partial \mathbf{q}}{\partial t} + \nabla_d \mathbf{G} + \mathbf{B}\left(\nabla_d \mathbf{F}\right) = \mathbf{H}\left(\mathbf{q}\right), \tag{1}$$

$$\mathbf{q} = \left[\rho_1, \rho_2, \rho_1 \boldsymbol{v}_1, \rho_2 \boldsymbol{v}_2, \rho_2 e_2, \rho_1 E_1 + \rho_2 K_2\right]^{\mathrm{T}},$$

$$\mathbf{G} = \left[\rho_1 \boldsymbol{v}_1, \rho_2 \boldsymbol{v}_2, \rho_1 \boldsymbol{v}_1 \boldsymbol{v}_1, \rho_2 \boldsymbol{v}_2 \boldsymbol{v}_2, \rho_2 e_2 \boldsymbol{v}_2, \rho_1 E_1 \boldsymbol{v}_1 + \rho_2 K_2 \boldsymbol{v}_2\right]^{\mathrm{T}},$$

$$\mathbf{F} = \left[0, 0, p, p, 0, p\left(\alpha_1 \boldsymbol{v}_1 + \alpha_2 \boldsymbol{v}_2\right)\right]^{\mathrm{T}}, \quad \mathbf{H} = \left[0, 0, -\mathbf{F}_\mu, \mathbf{F}_\mu, Q_T, -Q_T\right]^{\mathrm{T}},$$

$$\nabla_d = \mathrm{diag}\left(\nabla\cdot, \nabla\cdot, \nabla, \nabla, \nabla\cdot, \nabla\cdot\right), \quad \mathbf{B} = \mathrm{diag}\left[1, 1, \alpha_1, \alpha_2, 1, 1\right],$$

$$\rho_i = \rho_i^\circ \alpha_i, \quad \alpha_1 + \alpha_2 = 1, \quad E_i = e_i + K_i, \quad K_i = \boldsymbol{v}_i^2/2, \quad i = 1, 2.$$

Here the lower indices 1 and 2 at the bottom refer to the carrier and dispersed phase parameters, respectively; ∇ is the Hamiltonian operator. By $\alpha_i, \rho_i^\circ, \rho_i, \boldsymbol{v}_i, E_i, e_i, K_i$, and p we denote the volume fraction, true and reduced densities, velocity vector, total, internal and kinetic energies of unit mass of the ith phase, and the gas pressure; $\mathbf{F}_\mu$ and Q_T are the viscous component of the interphase interaction force and the heat exchange capacity between the gas and the particles per unit volume; and t is time.

The constitutive equations of system (1) are the equations of state of ideal calorically perfect gas and incompressible solid particles: $p = (\gamma_1 - 1)\rho_1^\circ e_1$, $e_1 = c_v T_1$, $e_2 = c_2 T_2$, $\{\gamma_1, c_v, c_2, \rho_2^\circ\} \equiv \mathrm{const}$, where T_1 and T_2 are the temperatures of the carrier phase and the particles; γ_1 and c_v is the ratio of specific heats or the adiabatic exponent and the specific heat capacity of the gas at constant volume; and c_2 is the specific heat capacity of the particles. The force and thermal phase interactions $\mathbf{F}_\mu$ and Q_T can be found by the formulas [38]

$$\mathbf{F}_\mu = (3/8)(\alpha_2/r)C_\mu \rho_1 \boldsymbol{w}_{12}\left|\boldsymbol{w}_{12}\right|, \qquad \boldsymbol{w}_{12} = \boldsymbol{v}_1 - \boldsymbol{v}_2, \qquad Q_T = (3/2)(\alpha_2/r^2)\lambda_1 \mathrm{Nu}_1(T_1 - T_2).$$

Here r is the particle radius, λ_1 is the thermal conductivity of the gas, C_μ and Nu_1 are the drag coefficient and the Nusselt number determined empirically [38].

3. Hybrid large-particle method. Here we briefly describe the algorithm of the hybrid large-particle method [39] for a one-dimensional case; its generalization to spatial orthogonal meshes is fulfilled without significant difficulties. A uniform grid with cell size h is used in the calculations. The integer indices refer to the center of the cell x_n, whereas the half-integer indices refer to its faces $x_{n\pm 1/2} = x_n \pm h/2$. The time layer t^k is numbered by the upper index k, whereas the time step is denoted by $\tau = t^{k+1} - t^k$.

The algorithm consists of a *predictor* step splitted into Lagrangian (0), Eulerian and final (1) stages:

$$\mathbf{q}_n^{(0)} - \mathbf{H}\left(\mathbf{q}_n^{(0)}\right)\tau = \mathbf{q}_n^k - \mathbf{B}_n^k\left(\tilde{\mathbf{F}}_{n+1/2}^k - \tilde{\mathbf{F}}_{n-1/2}^k\right)\tau/h, \tag{2}$$

$$\mathbf{q}_n^{(1)} = \mathbf{q}_n^{(0)} - \left(\hat{\mathbf{G}}_{n+1/2}^{(0)} - \hat{\mathbf{G}}_{n-1/2}^{(0)}\right)\tau/h, \tag{3}$$

and the *corrector* step to determine the final values of the sought functions with $O\left(h^2 + \tau^2\right)$ total approximation on smooth solutions:

$$\mathbf{q}_n^{(2)} - 0.5\mathbf{H}\left(\mathbf{q}_n^{(2)}\right)\tau = 0.5\left(\mathbf{q}_n^k + \mathbf{q}_n^{(1)}\right) - 0.5\left(\tilde{\mathbf{F}}_{n+1/2}^{(1)} - \tilde{\mathbf{F}}_{n-1/2}^{(1)}\right)\tau/h, \tag{4}$$

$$\mathbf{q}_n^{k+1} = \mathbf{q}_n^{(2)} - 0.5\left(\hat{\mathbf{G}}_{n+1/2}^{(2)} - \hat{\mathbf{G}}_{n-1/2}^{(2)}\right)\tau/h. \tag{5}$$

Remark 1. In order to ensure the monotonicity of the numerical solution at the Lagrangian stage, a nonlinear artificial viscosity $Q_{n\pm1/2}$ with the Christensen limiter ψ_v [40] is introduced:

$$\tilde{p}_{n\pm1/2} = p_{n\pm1/2} + (1 - \psi_v)Q_{n\pm1/2}.$$

At the Eulerian stage, the hybrid flux scheme

$$\hat{\mathbf{G}}_{n\pm1/2} = (1 - \psi_f)\mathbf{G}_{n\pm1/2}^{\text{Upwind}} + \psi_f\mathbf{G}_{i\pm1/2}^{\text{Centered}}$$

with the limiter ψ_f is used.

Remark 2. The high stability of the scheme is achieved by the implicit accounting of the source terms $\mathbf{H}\left(\mathbf{q}_n\right)$ (interphase friction and heat transfer) [25]. In order to eliminate the iterative procedures, we use the $\mathbf{H}\left(\mathbf{q}_n\right)$ linearization and take into account the linear part implicitly [26].

The time step is determined from the Courant–Friedrichs–Lewy condition for a "pure" gas:

$$\tau^k = \text{CFL}\frac{h}{\max\limits_{\forall n}\left(|v_n^k| + a_{1,n}^k\right)},$$

where CFL is a fixed Courant number (its recommended value is $\leqslant 0.5$) and $a_{1,n}^k$ is the sound speed in the gas phase at the point $\left(x_n, t^k\right)$.

Our calculations were performed with the Courant number CFL = 0.4. For the nonlinear correction of the scheme, we use the Van Leer flux limiter $\psi_f = (r + |r|)/(1 + r)$ in (3) and (5) and the Superbee viscosity limiter $\psi_v = \max\left[\min\left(2r, 1\right), \min\left(r, 2\right), 0\right]$ in (2) and (4), where r is the ratio of the parameter's inclinations at the cell face [41].

4. Equilibrium solutions. We assume that the flow is equilibrium with respect to velocities $u = u_1 = u_2$ and phase temperatures $T = T_1 = T_2$. This assumption is true when the phase relaxation times are much smaller than the time scale of the problem. Suppose the two-phase medium flow is characterized by constant parameters on the left $(p_L, u_L, \rho_L, \alpha_{1L})$ and on the right $(p_R, u_R, \rho_R, \alpha_{1R})$ of an arbitrary discontinuity for $x = x_c$ and $t = t_c$, and also for $p_L > p_R$ and $u_R = 0$. Let us write out the formulas derived from the basic relations [42, 43] to define the arbitrary discontinuity decomposition (Riemann problem) in an equilibrium two-phase medium.

In the case $u_L \geqslant u'$, where

$$u' = (p_L - p_R)\sqrt{\frac{\chi_L - 1}{\rho_R\left(\kappa_L p_L + p_R\right)}},$$

a configuration with two shock waves (SS) with pressure P, velocity U and mixture densities R_- and R_+ to the left and to the right of the contact discontinuity is realized. First, the pressure P is found:

$$u_L - (P - p_L)\sqrt{\frac{\chi_L - 1}{\rho_L\left(\kappa_L P + p_L\right)}} = (P - p_R)\sqrt{\frac{\chi_R - 1}{\rho_R\left(\kappa_R P + p_R\right)}}.$$

Here $\chi_J = \left(\gamma_J^* + 2\alpha_{1J} - 1\right)/\left(\gamma_J^* - 1\right)$, $\kappa_J = \left(\gamma_J^* + 1\right)/\left(\gamma_J^* - 1\right)$ are auxiliary functions, J is the area index (L or R), $\gamma^* = 1 + \left(\zeta_1 R_1\right)/\left(\zeta_1 c_v + \zeta_2 c_2\right)$ is the mixture polytropic exponent, $\zeta_i = \rho_i/\rho$ are the mass concentrations of phases, and R_1 is the gas constant. Then, the other parameters are found:

$$U = u_L - (P - p_L)\sqrt{\frac{\chi_L - 1}{\rho_L\left(\kappa_L P + p_L\right)}},$$

$$R_- = \rho_L\frac{\kappa_L P + p_L}{\chi_L p_L + \dfrac{\gamma_L^* - 2\alpha_{1L} + 1}{\gamma_L^* - 1}P}, \qquad \alpha_{1-} = 1 - \frac{R_-}{\rho_L}(1 - \alpha_{1L}),$$

$$R_+ = \rho_R \frac{\kappa_R P + p_R}{\chi_R p_R + \dfrac{\gamma_R^* - 2\alpha_{1R} + 1}{\gamma_R^* - 1} P}, \qquad \alpha_{1+} = 1 - \frac{R_+}{\rho_R}\left(1 - \alpha_{1R}\right).$$

Using the obtained gas dynamic quantities, we can determine the Mach number and the velocities for the left and right shock waves:

$$\mathrm{M}_- = \sqrt{\frac{\alpha_{1L}}{\alpha_{1-}}\left(\frac{\gamma_L^* + 2\alpha_{1-} - 1}{2\gamma_L^*}\frac{P}{p_L} + \frac{\gamma_L^* - 2\alpha_{1-} + 1}{2\gamma_L^*}\right)}, \qquad D_- = u_L - \mathrm{M}_- a_L,$$

$$\mathrm{M}_+ = \sqrt{\frac{\alpha_{1R}}{\alpha_{1+}}\left(\frac{\gamma_R^* + 2\alpha_{1+} - 1}{2\gamma_R^*}\frac{P}{p_R} + \frac{\gamma_R^* - 2\alpha_{1+} + 1}{2\gamma_R^*}\right)}, \qquad D_+ = \mathrm{M}_+ a_R,$$

where $a_J = \sqrt{\gamma_J^* p_J / \left(\rho_J \alpha_J\right)}$ is the sound speed in the domain J.

In the case of $u'' \leqslant u_L < u'$, where

$$u'' = \frac{2 a_L \alpha_L}{\gamma_L^* - 1}\left[1 - \left(\frac{p_R}{p_L}\right)^{\frac{\gamma_L^* - 1}{2\gamma_L^*}}\right],$$

a configuration is formed with a rarefaction wave, a region of constant flow, a contact discontinuity, and a shock wave (WS). The pressure P is determined as a solution to the equation

$$u_L + \frac{2 a_L \alpha_{1L}}{\gamma_L^* - 1}\left[1 - \left(\frac{P}{p_L}\right)^{\frac{\gamma_L^* - 1}{2\gamma_L^*}}\right] = (P - p_R)\sqrt{\frac{\chi_R - 1}{\rho_R P + p_R}}.$$

We also determine the other parameters behind the shock wave (marked by "+") and in the constant flow zone between the contact discontinuity and the rarefaction wave (marked by "−"):

$$U = (P - p_R)\sqrt{\frac{\chi_R - 1}{\rho_R\left(\kappa_R P + p_R\right)}},$$

$$R_+ = \rho_R \frac{\kappa_R P + p_R}{\chi_R p_R + \dfrac{\gamma_R^* - 2\alpha_{1R} + 1}{\gamma_R^* - 1} P}, \qquad \alpha_{1+} = 1 - \frac{R_+}{\rho_R}\left(1 - \alpha_{1R}\right),$$

$$R_- = \rho_L\left[\alpha_{2L} + \alpha_{1L}\left(1 - \frac{\gamma_L^* - 1}{2\alpha_{1L}}\frac{U - u_L}{a_L}\right)^{-\frac{2}{\gamma_L^* - 1}}\right]^{-1}, \qquad \alpha_{1-} = 1 - \frac{R_-}{\rho_L}\left(1 - \alpha_{1L}\right),$$

$$\mathrm{M}_+ = \sqrt{\frac{\alpha_{1R}}{\alpha_{1+}}\left(\frac{\gamma_R^* + 2\alpha_{1+} - 1}{2\gamma_R^*}\frac{P}{p_R} + \frac{\gamma_R^* - 2\alpha_{1+} + 1}{2\gamma_R^*}\right)}, \qquad D_+ = \mathrm{M}_+ a_R.$$

In the centered rarefaction wave region $u_L - a_L \leqslant (x - x_c)/(t - t_c) \leqslant U - a_+$, the solution is self-similar, depending on the variable $\xi' = \dfrac{x - x_c}{a_L \alpha_{1L}\left(t - t_c\right)} - \dfrac{\mathrm{M}_L'}{\alpha_{1L}}$:

$$\left[\frac{\left(1 - \alpha_{1L}\right)\alpha_1}{\left(1 - \alpha_1\right)\alpha_{1L}}\right]^{\omega} = \frac{\alpha_1 + \omega}{\alpha_1\left(1 - \omega\xi'\right)}, \qquad \omega = \frac{\gamma_L^* - 1}{2},$$

$$\mathrm{M}' = \mathrm{M}_L' + \frac{2\alpha_{1L}}{\gamma_L^* + 2\alpha_1 - 1}\left(\alpha_1 \xi' + 1\right), \quad \mathrm{M}' = \frac{u}{a_L}, \quad \mathrm{M}_L' = \frac{u_L}{a_L},$$

$$\rho = \rho_L \frac{\alpha_1}{\alpha_{1L}}\left(1 - \frac{\gamma_L^* - 1}{2\alpha_L}\left(\mathrm{M}' - \mathrm{M}_L'\right)\right)^{\frac{1}{\omega}}, \quad p = p_L\left(1 - \frac{\gamma_L^* - 1}{2\alpha_L}\left(\mathrm{M}' - \mathrm{M}_L'\right)\right)^{\frac{\gamma_L^*}{\omega}}.$$
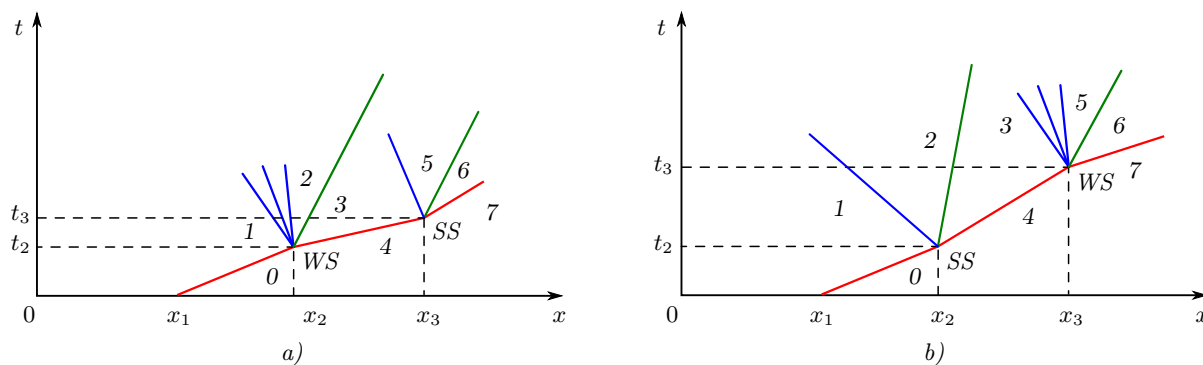
Figure 1. Shock wave interaction with a gas suspension layer:
a) lower density, *b)* higher density

Remark 3. For completeness, we formulate the condition for the fulfillment of the third case (two rarefaction waves WW): $u''' \leqslant u_L < u''$, where $u''' = -\dfrac{2a_L\alpha_L}{\gamma_L^* - 1} - \dfrac{2a_R\alpha_R}{\gamma_R^* - 1}$.

Remark 4. When deriving the formulas for discontinuity decomposition, we use the property of conservation of phase mass concentrations along the mixture trajectory $d\zeta_2/dt \equiv \partial\zeta_2/\partial t + u\partial\zeta_2/\partial x = 0$ and, consequently, the invariance of the mixture polytropic exponent $d\gamma^*(\zeta_2)/dt = 0$. From here, we come to the equalities $\gamma_-^* = \gamma_L^*$ and $\gamma_+^* = \gamma_R^*$.

Remark 5. The relations described above represent an asymptotically exact solution of the Riemann problem for the full equations (1) of gas suspension dynamics as the particle diameter decreases: $d \to 0$.

Now we consider a one-dimensional version of interaction between a shock wave and a step of lower density (case 1) or a step of higher density (case 2). The interaction of the shock wave whose Mach number is $\mathrm{M}_0 = 1.22$ with heterogeneities located in the region $x_2 \leqslant x \leqslant x_3$ is illustrated in the x–t diagram (Fig. 1, the shock wave trajectories and the rarefaction wave characteristics are shown in red and blue, respectively, and the contact discontinuity trajectories are shown in green).

The flow is characterized by the initial state *0*, *4* and *7* as well as by the parameters behind the incident shock wave *1* refracted in layer *3* and passing through *6* and behind the reflected centered rarefaction wave *2* (the case of lower density) or *5* (the case of higher density). When an incident shock wave interacts with the step considered above, two types of discontinuities occur: rarefaction wave–shock wave WS or two shock waves SS (see the above computational relations).

The one-dimensional problems were solved with the initial conditions shown in Table 1.

The boundary conditions on the left and right are prescribed in the form of free inflow and outflow. For the homogeneity of the algorithm, a negligibly small particle concentration $\alpha_2 = 10^{-10}$ was specified in the "pure" gas region. The parameters behind the incident shock wave (region *1*, Fig. 1) were determined by the following relations [30]:

$$\mathrm{M}_0^2 = \frac{\alpha_{10}}{\gamma_0^*} \frac{[\chi_0(\alpha_{20}) + 1]\alpha_{21} - [\chi_1(\alpha_{21}) + 1]\alpha_{20}}{\chi_1(\alpha_{21})\alpha_{20} - \alpha_{21}} \frac{\alpha_{21}}{\alpha_{21} - \alpha_{20}},$$

Table 1

Initial conditions for one-dimensional problems (SI measurements)

| Domain of definition	$(\alpha_2, p, T_1, T_2, u_1, u_2)$
before the shock wave $x_1 < x < x_2$ и $x > x_3$	$(0.001, 1.01325 \cdot 10^5, 293.23, 293.23, 0, 0)$ case 1 $(10^{-10}, 1.01325 \cdot 10^5, 293.23, 293.23, 0, 0)$ case 2
behind the shock wave $x < x_1$	$(1.44442 \cdot 10^{-3}, 1.53851 \cdot 10^5, 308.111, 308.111, 66.0650, 66.0650)$ case 1 $(1.37636 \cdot 10^{-10}, 1.5906 \cdot 10^5, 334.441, 334.441, 114.51, 114.51)$ case 2
heterogeneity $x_2 < x < x_3$	$(10^{-10}, 1.01325 \cdot 10^5, 293.23, 293.23, 0, 0)$ case 1 $(0.001, 1.01325 \cdot 10^5, 293.23, 293.23, 0, 0)$ case 2
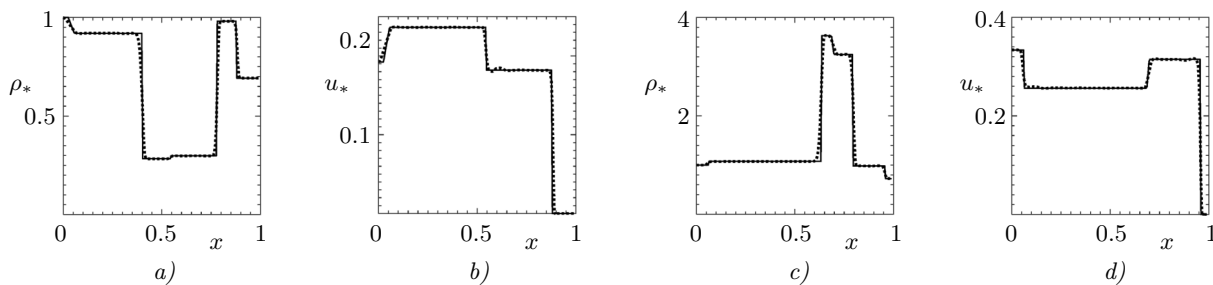
Figure 2. Distributions of relative values of density ρ_* and velocity u_*
of gas suspension at the time instant $t = 0.001$ s

$$\rho_1 = \rho_0 \frac{\alpha_{21}}{\alpha_{20}}, \qquad p_1 = p_0 \frac{\chi_0\left(\alpha_{20}\right)\alpha_{21} - \alpha_{20}}{\chi_1\left(\alpha_{21}\right)\alpha_{20} - \alpha_{21}}, \qquad u_1 = \sqrt{\frac{p_1 - p_0}{\rho_0}\frac{\alpha_{10} - \alpha_{11}}{1 - \alpha_{11}}}.$$

In order to compare the numerical and analytical solutions, calculations were performed by the hybrid large-particle method using the full equations (1) of non-equilibrium gas suspension dynamics in the shock-wave refraction problem on the heterogeneities of lower or higher density. The results in the form of distributions of relative values of density $\rho_* = \rho/\rho_1$ and velocity $u_* = u/a_0$ of the mixture of air and silica sand particles with true density $\rho_2^\circ = 2500$ kg/m^3 are illustrated in Fig. 2 (a, b for case 1; c, d for case 2). Here the solid lines correspond to the exact solutions, whereas the dashed curves correspond to calculations for sufficiently fine particles $d = 0.1\ \mu$m on the 1/200 grid with the grid step $h = 2$ mm. The computation final time is $t = 0.001$ s.

The numerical results are found to be in good agreement with the self-similar solutions. When the grid resolution is increased to 1/400, the calculated and analytical curves graphically coincide, the relative discrepancy is of the order 10^{-4} at the characteristic points 0.3 and 0.7.

Of practical interest is the degree of shock wave attenuation in air when this shock wave passes through the gas suspension layer, depending on the Mach number M_0 and the volume concentration of the dispersed phase in the heterogeneity $\alpha_s = \alpha_{24}$ (the indices correspond to the regions shown in Fig. 1b). The numerical results obtained by the analytical relations for an equilibrium two-phase medium are shown in Fig. 3a and b, where the dependencies of the shock wave attenuation $p_* = p_6/p_1$ and the dependences of the maximum gas suspension layer compression $\alpha_* = \alpha_{23}$ on M_0 are calculated for a fixed value of the initial volume fraction $\alpha_s = 0.001$ of particles in the layer. The fixed Mach number $M_0 = 1.5$ of the incident shock wave is given in Fig. 3 c, d. The parameters p_* and α_* were determined depending on the initial volume concentration α_s of the dispersed phase of the gas suspension layer.

As the Mach number increases, the compression of the gas suspension layer and the attenuation of the incident shock wave also increase (Fig. 3 a and b), which can be explained by a more intense absorption of the shock wave impulse by the mixture. As the initial particle concentration increases, so does the attenuation of the incident shock wave; the intensity of the passed wave is about 30% lower in relation to the initial shock wave for $\alpha_s = 0.01$ (Fig. 3 c). In this case, the layer compression is almost linear (Fig. 3 d).

5. A discussion of numerical two-dimensional solutions. Let's consider a flat two-dimensional channel 1 (Fig. 4) with a stationary shock wave 2 moving in air with the Mach number 1.22 and interacting with a
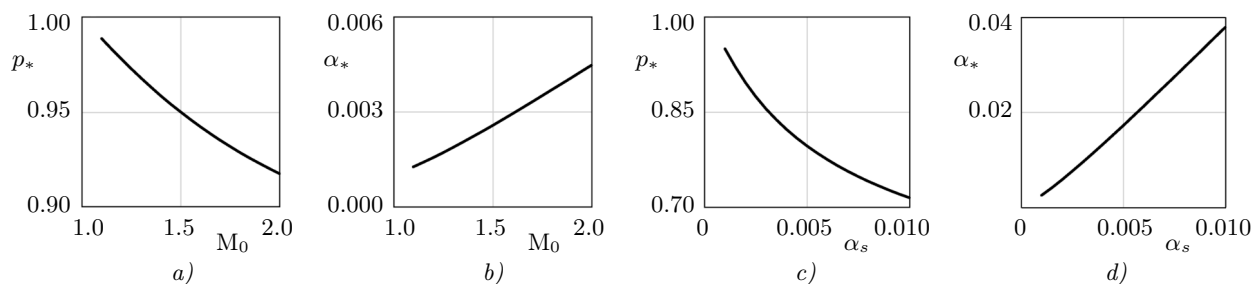

Figure 3. Analytical dependencies of the shock wave attenuation degree p_* and the maximum gas
suspension layer compression value α_* depending: a), b) on the Mach number M_0 for $\alpha_s = 0.001$;
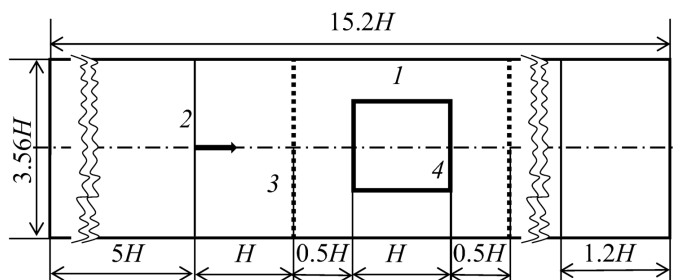c), d) on the initial volume concentration α_s of particles for $M_0 = 1.5$

Figure 4. Computational scheme

Initial conditions for the two-dimensional problems (SI measurements)

Domain of definition	$(\alpha_2, p, T_1, T_2, u_1, u_2)$
before the shock wave	$\left(10^{-10}, 1.01325 \cdot 10^5, 293.23, 293.23, 0, 0\right)$
behind the shock wave	$\left(1.37636 \cdot 10^{-10}, 1.5906 \cdot 10^5, 334.441, 334.441, 114.51, 114.51\right)$
gas suspension layer	$\left(0.001, 1.01325 \cdot 10^5, 293.23, 293.23, 0, 0\right)$ case 1 $\left(0.0001, 1.01325 \cdot 10^5, 293.23, 293.23, 0, 0\right)$ case 2
heterogeneity	$\left(10^{-10}, 1.01325 \cdot 10^5, 293.23, 293.23, 0, 0\right)$ case 1 $\left(0.001, 1.01325 \cdot 10^5, 293.23, 293.23, 0, 0\right)$ case 2

limited layer of gas suspension *3*; in the layer, there is a square heterogeneity *4* with a lower (case 1) or higher (case 2) density.

The initial conditions of two-dimensional problems are presented in Table 2.

The incompressible gas suspension particles have the density $\rho_2^\circ = 2500$ kg/m^3 and the specific heat capacity $c_2 = 710$ J/(kg$\cdot$K).

The boundary conditions are specified as reflections on the walls and as free inflow and outflow on the left and right of the computational domain. Calculations were performed up to the symmetry axis on a uniform grid with a resolution of 200 cells per the heterogeneity size $H = 5$ cm up to the time instant $t_f = 2.5$ ms. In the right side of the computational domain with the size $1.2\,H$, we use a non-uniform grid with the cell step h varying according to the dependence $h'_{n+1} = h'_n + 0.5h$ (where n is the cell number).

First we consider the interaction between a shock wave and a gas suspension layer with a fine fraction $d = 0.1$ μm of particles. In this case, the flow of the mixture is close to equilibrium. The spatial relaxation zones are sub-grid. The gas suspension behaves as a "heavy" gas with the special equation $e = p\alpha_1 / \left[(\gamma^* - 1)\, \rho \right]$ of state (where e is the internal energy of the mixture) [42, 43].

Figures 5 and 6 illustrate, respectively, the numerical solutions obtained for the heterogeneities with lower and higher densities in the form of Schlieren images of the mixture density gradient function. Four characteristic time instants are shown in these figures. After colliding the incident shock wave with the left boundary c_1 of the gas suspension layer, the discontinuity disintegration is observed with the reflected and passing shock waves s_1. When interacting the shock wave with the heterogeneity, then, there appear the WS-type (Fig. 5 *a*) or SS-type decomposition (Fig. 6 *a*). The structures are formed, known as the von Neumann double refraction: with a passing shock wave s_2, a precursor, a Mach stem, and two curved shock waves (see N_1 in Fig. 5 *a* and N_2 in Fig.6 *a*). Due to the different sound speeds in the heterogeneity and gas suspension layer, the shock wave s_2 lags behind (in case 1) or is ahead (in case 2) of the external shock wave s_1.

When the shock waves s_3 and s_4 move to the symmetry axis, the reflected waves s_5 and the focusing effect f are observed in the higher-density heterogeneity problem (Fig. 6 *b* and *c*). In case 1, the motion of the shock waves s_4 is of a divergent nature (Fig. 5 *b* and *c*). At the time instants being considered, the curvature of the gas suspension layer surfaces is observed with the convexity along the flow for case 1 and against the flow for case 2. After that, the contact boundaries c_1 and c_2 of the gas suspension layer are significantly deformed and the Richtmyer-Meshkov instability as well as the turbulent multidirectional mushroom vortex structures tu are developed (Fig. 5 *d* and Fig. 6 *d*).

As the gas suspension particles increase in size, the non-equilibrium effect (a difference in the velocities
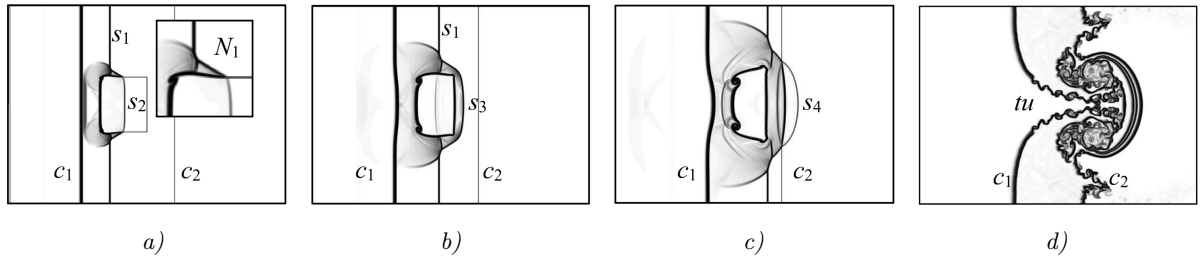
Figure 5. Shock wave interaction with the lower-density heterogeneity ($d = 0.1$ μm). The numerical Schlieren images of the mixture density gradient function at the time instants: *a)* 0.3 ms; *b)* 0.4 ms; *c)* 0.5 ms; *d)* 2.5 ms
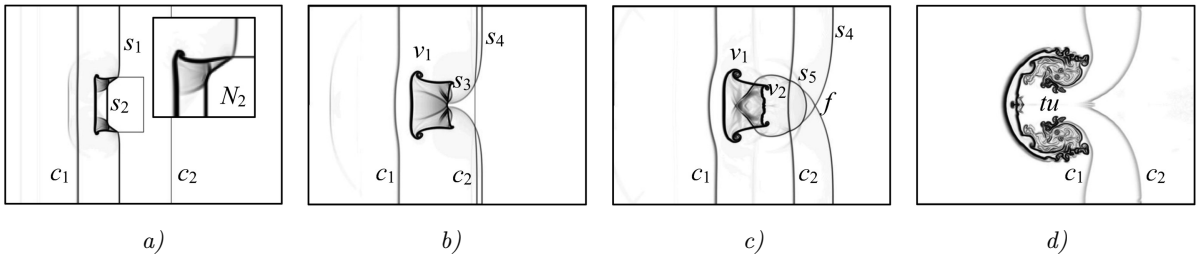

Figure 6. Shock wave interaction with the higher-density heterogeneity ($d = 0.1$ μm). The numerical Schlieren images of the mixture density gradient function at the time instants: *a)* 0.26 ms; *b)* 0.4 ms; *c)* 0.5 ms; *d)* 2.5 ms

and temperatures of phases) begins to appear. Figure 7 shows the Schlieren images of the mixture density gradient function as well as the distributions of the relative mixture density $\bar{\rho} = \rho/\rho_1$ on the symmetry axis for the particle diameters $d = 0.1$, 1, 2, 10 μm at the time instant $t = 0.26$ ms for case 2. The axial coordinate is related to the size $\bar{x} = x/H$ of the heterogeneity.

The relaxation processes for the mixture of a carrier gas and a group of particles are characterized by the phase velocity and temperature equalization times [31]. Since their values are comparable in order for the problem under consideration, we use the dynamic relaxation time of the disperse phase $t_2^{(\mu)} = \rho_2^\circ d^2 / (18\mu_1 \alpha_1)$
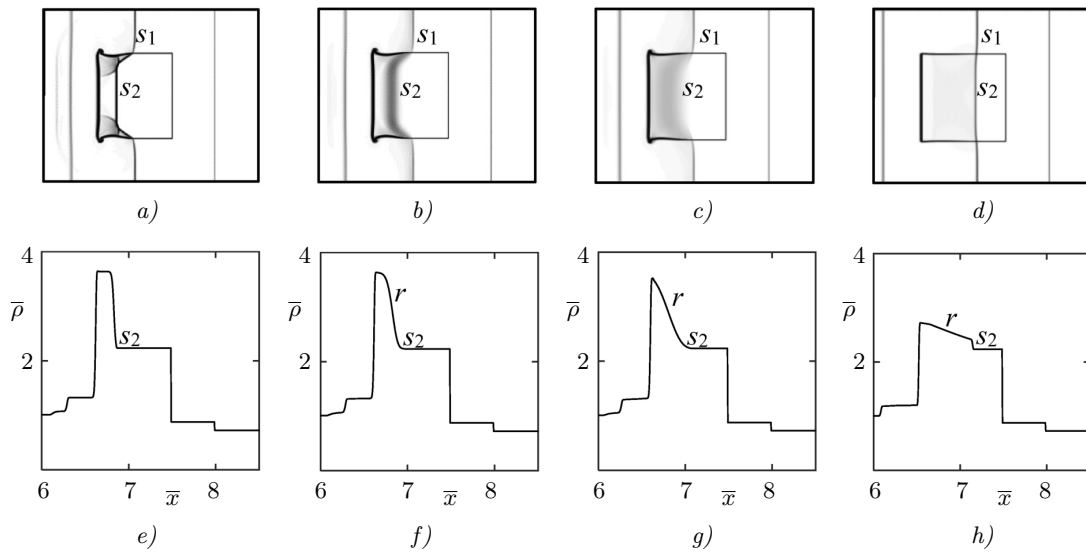

Figure 7. Interaction of a shock wave with a higher density heterogeneity at the time instant $t = 0.26$ ms. The numerical Schlieren images of mixture density gradient function as well as the distributions of mixture density on the symmetry axis for the particle diameters: *a), e)* 0.1 μm; *b), f)* 1 μm; *c), g)* 2 μm; *d), h)* 10 μm

as a scale. The expression $\bar{h}_r = \left(a_{10}\, 3\, t_2^{(\mu)}\right)/H$ can be considered as a good approximation for estimating the relative spatial relaxation zone behind the shock wave; here a_{10} is the sound speed in the carrier gas. For the studied range of particle sizes, the values of $\bar{h}_r$ are equal to 0.0016, 0.16, 0.64, and 16, which corresponds to the computational domains of the mixture density profile "smearing" (Fig. 7). The structural features of the gas suspension flow are characterized by two strong discontinuities s_1 and s_2 for $d = 0.1$ μm (Fig. 7 a and e), by a strong discontinuity for the shock wave envelope s_1 in the gas suspension layer, by a deteriorated (sound) wave front in the heterogeneity s_2 for $d = 1$ and 2 μm (Fig. 7 b, c, f, g), and by two shock waves s_1 and s_2 of finite intensity for $d = 10$ μm (Fig. 7 d and h).

6. Conclusion. Asymptotically exact equilibrium solutions are obtained for a one-dimensional formulation of the problem on the shock wave interaction with regions of lower or higher density. Our numerical results obtained by the large-particle hybrid method using the non-equilibrium dynamic equations for a mixture of gas and solid particles are in good agreement with the asymptotic solutions. The analysis of shock wave attenuation by a layer of fine gas suspension for different Mach numbers and dispersed phase concentrations in the heterogeneity is performed on the basis of self-similar relations.

The heterogeneous layer dynamics during the passage of a shock wave in two-dimensional regions is studied. An estimate of the spatial relaxation zones for different particle sizes is obtained; this estimate is consistent with our numerical simulation results. It was found that, depending on phase relaxation times, two flow modes are realized: with two strong discontinuities or with the shock wave envelope together with a degenerate (sound) wave front inside the heterogeneity.

The large-particle hybrid method shows a large stability margin and high resolution capability for detecting the shock wave structures and the formation of Richtmyer-Meshkov instabilities. The method is universal and allows solving an extended class of convection dominated problems of hyperbolic or mixed type in conservative or non-divergent notation of equations. The problems we considered along with asymptotically exact solutions can serve as a test for testing other difference schemes.

References

1. B. L. Rozhdestvenskii and N. N. Yanenko, *Systems of Quasilinear Equations and Their Applications to Gas Dynamics* (Nauka, Moscow, 1978; Amer. Math. Soc., Providence, 1982).

2. G. A. Ruev, B. L. Rozhdestvenskii, V. M. Fomin, and N. N. Yanenko, "Conservation Laws for Systems of Equations for Two-Phase Media," Dokl. Akad. Nauk SSSR **254** (2), 288–293 (1980) [Sov. Math. Dokl. **22** (2), 352–357 (1980)].

3. L. Huilin, D. Gidaspow, J. Bouillard, and L. Wentie, "Hydrodynamic Simulation of Gas–Solid Flow in a Riser Using Kinetic Theory of Granular Flow," Chem. Eng. J. **95** (1–3), 1–13 (2003).

4. K. N. Volkov, V. N. Emelyanov, A. G. Karpenko, and I. V. Teterina, "Simulation of Unsteady Gas–Particle Flow Induced by the Shock-Wave Interaction with a Particle Layer," Vychisl. Metody Programm. **21** (1), 96–114 (2020).

5. R. Saurel and R. Abgrall, "A Multiphase Godunov Method for Compressible Multifluid and Multiphase Flows," J. Comput. Phys. **150** (2), 425–467 (1999).

6. R. Abgrall and R. Saurel, "Discrete Equations for Physical and Numerical Compressible Multiphase Mixtures," J. Comput. Phys. **186** (2), 361–396 (2003).

7. S. A. Tokareva and E. F. Toro, "HLLC-Type Riemann Solver for the Baer–Nunziato Equations of Compressible Two-Phase Flow," J. Comput. Phys. **229** (10), 3573–3604 (2010).

8. R. Jackson, "The Mechanics of Fluidized Beds. I: The Stability of the State of Uniform Fluidization," Trans. Inst. Chem. Eng. **41**, 13–21 (1963).

9. G. Rudinger and A. Chang, "Analysis of Non-Steady Two-Phase Flow," Phys. Fluid **7**, 1747–1754 (1964).

10. R. I. Nigmatulin, *Fundamentals of the Mechanics of Heterogeneous Media* (Nauka, Moscow, 1978) [in Russian].

11. C. K. K. Lun, S. B. Savage, D. J. Jeffrey, and N. Chepurniy, "Kinetic Theories for Granular Flow: Inelastic Particles in Couette Flow and Slightly Inelastic Particles in a General Flowfield," J. Fluid Mech. **140**, 223–256 (1984).

12. J. Ding and D. Gidaspow, "A Bubbling Fluidization Model Using Kinetic Theory of Granular Flow," AIChE J. **36** (4), 523–538 (1990).

13. A. Boemer, H. Qi, and U. Renz, "Eulerian Simulation of Bubble Formation at a Jet in a Two-Dimensional Fluidized Bed," Int. J. Multiph. Flow **23** (5), 927–944 (1997).

14. M. A. Gol'dshtik, "Elementary Theory of the Boiling Layer," Zh. Prikl. Mekh. Tekh. Fiz., No. 6, 106–112 (1972) [J. Appl. Mech. Tech. Phys. **13** (6), 851–856 (1972)].

15. D. V. Sadin, "Behavior of the Unsteady Jet of a Mixture of a Pressurized Gas and Dispersed Particles Discharged from a Circular Duct into the Atmosphere," Zh. Prikl. Mekh. Tekh. Fiz., **40** (1), 151–157 (1999) [J. Appl. Mech. Tech. Phys. **40** (1), 130–135 (1999)].

16. D. V. Sadin, S. D. Lyubarskii, and Yu. A. Gravchenko, "Features of an Underexpanded Pulsed Impact Gas-Dispersed Jet with a High Particle Concentration," Zh. Tekh. Fiz. **87** (1), 22–26 (2017) [Tech. Phys. **62** (1), 18–23 (2017)].

17. D. Gidaspow, *Multiphase Flow and Fluidization: Continuum and Kinetic Theory Descriptions* (Academic Press, New York, 1994).

18. A. Goldshtein and M. Shapiro, "Mechanics of Collisional Motion of Granular Materials. Part 1. General Hydrodynamic Equations," J. Fluid Mech. **282**, 75–114 (1995).

19. R. W. Lyczkowski, D. Gidaspow, C. W. Solbrig, and E. D. Hughes, "Characteristics and Stability Analyses of Transient One-Dimensional Two-Phase Flow Equations and Their Finite Difference Approximations," Nucl. Sci. Eng. **66** (3), 378–396 (1978).

20. L. A. Klebanov, A. E. Kroshilin, B. I. Nigmatulin, and R. I. Nigmatulin, "On the Hyperbolicity, Stability and Correctness of the Cauchy Problem for the System of Equations of Two-Speed Motion of Two-Phase Media," Prikl. Mat. Mech. **46** (1), 83–95 (1982) [J. Appl. Math. Mech. **46** (1), 66–74 (1982)].

21. D. A. Drew, "Mathematical Modelling of Two-Phase Flow," Ann. Rev. Fluid Mech. **15**, 261–291 (1983).

22. V. S. Surov, "Hyperbolic Models in the Mechanics of Heterogeneous Media," Zh. Vychisl. Mat. Mat. Fiz. **54** (1), 139–148 (2014) [Comput. Math. Math. Phys. **54** (1), 148–157 (2014)].

23. M. Hantke, C. Matern, and G. Warnecke, "Numerical Solutions for a Weakly Hyperbolic Dispersed Two-Phase Flow Model," in *Theory, Numerics and Applications of Hyperbolic Problems I* (Springer, Cham, 2018), Vol. 236, pp. 665–675.

24. D. V. Sadin, "On the Convergence of a Certain Class of Difference Schemes for the Equations of Unsteady Gas Motion in a Disperse Medium," Zh. Vychisl. Mat. Mat. Fiz. **38** (9), 1572–1577 (1998) [Comput. Math. Math. Phys. **38** (9), 1508–1513 (1998)].

25. D. V. Sadin, "A Modified Large-Particle Method for Calculating Unsteady Gas Flows in a Porous Medium," Zh. Vychisl. Mat. Mat. Fiz. **36** (10), 158–164 (1996) [Comput. Math. Math. Phys. **36** (10), 1453–1458 (1996)].

26. D. V. Sadin, "A Method for Computing Heterogeneous Wave Flows with Intense Phase Interaction," Zh. Vychisl. Mat. Mat. Fiz. **38** (6), 1033–1039 (1998) [Comput. Math. Math. Phys. **38** (6), 987–993 (1998)].

27. L. Gascón and J. M. Corberán, "Construction of Second-Order TVD Schemes for Nonhomogeneous Hyperbolic Conservation Laws," J. Comput. Phys. **172** (1), 261–297 (2001).

28. Y. Xing and C.-W. Shu, "High-Order Well-Balanced Finite Difference WENO Schemes for a Class of Hyperbolic Systems with Source Terms," J. Sci. Comput. **27** (1–3), 477–494 (2006).

29. R. Saurel, O. Le Métayer, J. Massoni, and S. Gavrilyuk, "Shock Jump Relations for Multiphase Mixtures with Stiff Mechanical Relaxation," Shock Waves **16** (3), 209–232 (2007).

30. D. V. Sadin, "TVD Scheme for Stiff Problems of Wave Dynamics of Heterogeneous Media of Nonhyperbolic Nonconservative Type," Zh. Vychisl. Mat. Mat. Fiz. **56** (12), 2098–2109 (2016) [Comput. Math. Math. Phys. **56** (12), 2068–2978 (2016)].

31. D. V. Sadin, "On Stiff Systems of Partial Differential Equations for Motion of Heterogeneous Media," Mat. Model. **14** (11), 43–53 (2002).

32. D. V. Sadin, "Stiffness Problem in Modeling Wave Flows of Heterogeneous Media with a Three-Temperature Scheme of Interphase Heat and Mass Transfer," Zh. Prikl. Mekh. Tekh. Fiz. **43** (2), 136–141 (2002) [J. Appl. Mech. Tech. Phys. **43** (2), 286–290 (2002)].

33. V. M. Bojko, V. P. Kiselev, S. P. Kiselev, et al., "Interaction of a Shock Wave with a Cloud of Particles," Fiz. Goreniya Vzryva **32** (2), 86–99 (1996) [Combust. Explos. Shock Waves **32** (2), 191–203 (1996)].

34. S. L. Davis, T. B. Dittmann, G. B. Jacobs, and W. S. Don, "Dispersion of a Cloud of Particles by a Moving Shock: Effects of the Shape, Angle of Rotation, and Aspect Ratio," Zh. Prikl. Mekh. Tekh. Fiz. **54** (6), 45–59 (2013) [J. Appl. Mech. Tech. Phys. **54** (6), 900–912 (2013)].

35. D. A. Tukmakov, "Numerical Study of Intense Shock Waves in Dusty Media with a Homogeneous and Two-Component Carrier Phase," Comput. Issled. Model. **12** (1), 141–154 (2020).

36. D. V. Sadin and V. A. Davidchuk, "Interaction of a Plane Shock Wave with Regions of Varying Shape and Density in a Finely Divided Gas Suspension," Inzh. Fiz. Zh. **93** (2), 489–498 (2020) [J. Eng. Phys. Thermophys. **93** (2), 474–483 (2020)].

37. K. N. Volkov, V. N. Emelyanov, A. G. Karpenko, and I. V. Teterina, "Two-Dimensional Effects on the Interaction of a Shock Wave with a Cloud of Particles," Vychisl. Metody Programm. **21**, 207–224 (2020).

38. R. I. Nigmatulin, *Dynamics of Multiphase Media* (Nauka, Moscow, 1987; Hemisphere, New York, 1990).

39. D. V. Sadin, "A Modification of the Large-Particle Method to a Scheme Having the Second Order of Accuracy in Space and Time for Shockwave Flows in a Gas Suspension," Vestn. Yuzhn. Ural. Gos. Univ. Ser. Mat. Model. Programm. **12** (2), 112–122 (2019).

40. R. B. Christensen, *Godunov Methods on a Staggered Mesh − An Improved Artificial Viscosity*, Preprint UCRL-JC-105269 (Lawrence Livermore Nat. Lab., Livermore, 1990).

41. C. Hirsch, *Numerical Computation of Internal and External Flows.* Vol. 2: *Computational Methods for Inviscid and Viscous Flows* (Wiley, New York, 1990).

42. D. V. Sadin, *Fundamentals of the Theory of Modeling Wave Heterogeneous Processes* (Mozhaisky Military Space Academy, St. Petersburg, 2000) [in Russian].

43. D. V. Sadin, "Stiff Problems of a Two-Phase Flow with a Complex Wave Structure," Fiz.-Khim. Kinetika Gaz Din. **15** (4) (2014). http://chemphys.edu.ru/issues/2014-15-4/articles/243/. Cited December 6, 2020.